INTERNATIONAL JOURNAL FOR NUMERICAL METHODS IN FLUIDS
Int. J. Numer. Meth. Fluids 2006; **50**:1–26
Published online 1 September 2005 in Wiley InterScience (www.interscience.wiley.com). DOI: 10.1002/fld.1015

Rotating incompressible flow with a pressure Neumann condition

Julio R. Claeyssen[1,*,†], Elba Bravo Asenjo[2] and Obidio Rubio[3]

[1]*IM-Promec, Universidade Federal do Rio Grande do Sul, P.O. Box 10673, 90001-970 Porto Alegre, RS—Brazil*
[2]*UNASP—Adventist University Center of São Paulo, SP—Brazil*
[3]*Facultad de Ciencias, Universidad Nacional de Trujillo, La Libertad—Peru*

SUMMARY

This work considers the internal flow of an incompressible viscous fluid contained in a rectangular duct subject to a rotation. A direct velocity–pressure algorithm in primitive variables with a Neumann condition for the pressure is employed. The spatial discretization is made with finite central differences on a staggered grid. The pressure and velocity fields are directly updated without any iteration. Numerical simulations with several Reynolds numbers and rotation rates were performed for ducts of aspect ratios 2:1 and 8:1. Copyright © 2005 John Wiley & Sons, Ltd.

KEY WORDS: incompressible flow; rotating duct; pressure Neumann condition; primitive variables

1. INTRODUCTION

This work seeks to investigate a variety of effects, through the numerical simulation of the internal flow of an incompressible viscous fluid contained in a rotating rectangular duct.

The Navier–Stokes equations, together with the free divergence condition, constitute the basic formulation for an incompressible flow. From a mathematical point of view, the system that governs this kind of flow is singular with respect to the pressure. There is no evolution equation for such quantity. Following the excellent work of Gresho and Sani [1], the pressure is obtained by solving a Poisson equation with a Neumann boundary condition. A compatibility condition of the source with the boundary conditions guarantees the existence of solutions.

A direct pressure–velocity algorithm with a pressure Neumann condition was successfully considered by the authors [2] with the driven cavity flow. This primitive variables algorithm allowed to update the pressure in one step without iteration. In this work, the effect of a

*Correspondence to: Julio R. Claeyssen, IM-Promec, Universidade Federal do Rio Grande do Sul, P.O. Box 10673, 90001-970 Porto Alegre, RS—Brazil.
†E-mail: julio@mat.ufrgs.br

Received 23 June 2003
Revised 24 January 2005
Accepted 31 January 2005

rotating force is incorporated to the above algorithm and in such a way that the use of central differences on a staggered grid allows to have second-order approximations [3, 4].

The internal rotating flow problem has been considered by several authors: Speziale [5, 6], Chen *et al*. [7], Robertson [4], Yang [8], Govatsos and Papantonis [9], among others. Speziale employed the divergence-vorticity formulation with finite-difference schemes due to Arakawa for the convective terms and the DuFort–Frankel scheme for the viscous-diffusion terms. Chen *et al*. employed Fourier–Chebyshev pseudo-spectral methods for solving incompressible flows in 3D channels in rotação with square traversal section. Robertson, performed numerical studies for laminar incompressible flows, in permanent regime, in curved ducts. He employed finite differences on a staggered grid with Newton method.

This work will be focused in the structure of the secondary flow and its effects on the flow in the axial direction of the duct. Here the axis of rotation is perpendicular to axial direction of the duct which is assumed to be long enough to suppress effects at the end. Consequently, the secondary flow is independent of the coordinate along the axial direction. The study was accomplished for ducts with aspect ratios 2:1 and 8:1. Several Reynolds numbers and rotation rates were considered. The results obtained exhibit a very good agreement with those found in the literature.

2. THE GOVERNING EQUATIONS

The equations that govern the flow of an incompressible viscous fluid are given by the momentum equation

$$\frac{\partial \mathbf{u}}{\partial t} + \mathbf{u}.\nabla\mathbf{u} + \nabla P = v\ \nabla^2\mathbf{u} + \mathbf{F} \quad \text{in } \Omega,\ t>0 \tag{1}$$

and the continuity equation

$$\nabla.\mathbf{u} = 0 \quad \text{in } \Omega,\ t>0 \tag{2}$$

In these equations, Ω is a spatial region limited by the contour Γ, v the kinematic viscosity, $\mathbf{u}=\mathbf{u}(t,\mathbf{x})$ and $P=P(t,\mathbf{x})$ are, respectively, the velocity and the pressure of the fluid and $\mathbf{F}$ is a forcing term.

The problem under consideration is a flow driven by the pressure of an incompressible viscous fluid contained in a rectangular duct subject to a permanent rotation in a perpendicular direction of the duct (Figure 1) [5, 10].

Here, the rotating vector, $\boldsymbol{\omega}=\omega j$ is in the direction of the y-axis, where ω is the angular velocity. We shall consider

$$\mathbf{F}(\mathbf{u}) = \frac{2}{Ro}\,\mathbf{j}\times\mathbf{u} \tag{3}$$

where $Ro = W_0/\omega D$ denotes the Rossby number for a length scale D and W_0 a velocity scale.

Equations (1) and (2) are subject to the following initial and boundary conditions:

$$\mathbf{u}(0,\mathbf{x}) = \mathbf{u}_0(\mathbf{x}), \quad \mathbf{x} \text{ in } \overline{\Omega} = \Omega\cup\Gamma \tag{4}$$

$$\mathbf{u} = \mathbf{u}_\Gamma(\mathbf{x},t) \quad \text{on } \Gamma = \partial\Omega \tag{5}$$

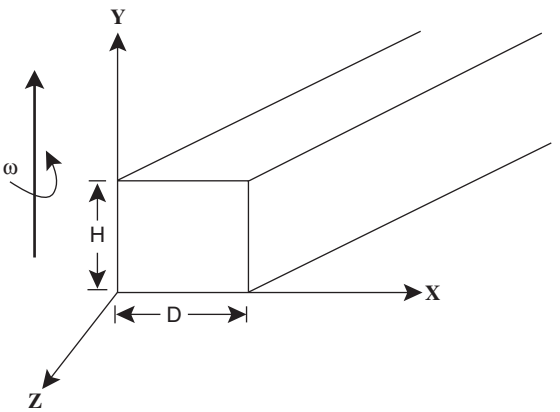

Figure 1. Flow in a rotating rectangular duct.

where $\mathbf{u}_0$ satisfies the continuity equation

$$\nabla.\mathbf{u}_0 = 0 \quad \text{in } \Omega \tag{6}$$

and $\mathbf{u}_0$, $\mathbf{u}_\Gamma$ being subject to the restriction

$$\mathbf{u}_0.n = \mathbf{u}_\Gamma(0,\mathbf{x}).n \quad \text{on } \Gamma \tag{7}$$

From the continuity equation and the divergence theorem, the condition of global mass follows:

$$\int_\Gamma \mathbf{u}.n \, \mathrm{d}x = 0 \tag{8}$$

where n is the unit exterior normal to the boundary Γ of the region Ω.

In agreement with Ladyzhenskaya [11], the specification of the pressure at the non-slip wall of Γ is not allowed. Otherwise, systems (1)–(7) would be overdetermined. It is clear from Equations (1)–(2), that there is no explicit equation for the pressure. The velocity field, in principle, calculated from the momentum equation must be restricted so that it satisfies the solenoidal cinematic condition $\nabla.\mathbf{u} = 0$. This means that the pressure influences twice. It not only serves as a force for conservation in the mechanical balance law but, also, as a continuity restriction [12].

2.1. The Poisson equation for the pressure

By applying the divergence operator in Equation (2), together with the momentum equation (1), lead us to the pressure equation

$$\nabla^2 P = \nabla.\left(\frac{1}{Re}\nabla^2\mathbf{u} - \mathbf{u}.\nabla\mathbf{u} + \mathbf{F}(\mathbf{u})\right) \quad \text{in } \Omega \text{ for } t \geqslant 0 \tag{9}$$

where $Re = W_0 D/v$ denotes the Reynolds number.

Thus, the pressure is determined by solving a Poisson equation subject to appropriate boundary conditions. For the problem being well-posed, the boundary conditions must be given in

such a way that the continuity equation be satisfied near the boundary. To keep the free-divergence condition for the velocity is an important requirement for the simulation of an incompressible flow.

The above equation is actually employed for substituting the continuity equation. The elliptic nature of this equation forces the need of prescribing a boundary condition for the pressure. In a fundamental work of Gresho and Sani [1], it is concluded that a Neumann condition for the pressure turns out to be the most appropriate. This condition is obtained by taking the normal component of the pressure gradient isolated from the momentum equation, that is

$$\frac{\partial P}{\partial n} = n.\nabla P = n.\left(\frac{1}{Re}\nabla^2\mathbf{u} - \frac{\partial \mathbf{u}}{\partial t} - \mathbf{u}.\nabla\mathbf{u} + \mathbf{F}(\mathbf{u})\right) \quad \text{on } \Gamma \text{ for } t \geqslant 0 \tag{10}$$

In order that a Poisson equation (9) with a Neumann condition (10) can be solved, it is necessary that the following compatibility condition be satisfied:

$$\iint_{\Omega} \nabla^2 P \, \mathrm{d}\Omega = \int_{\Gamma} P_n \, \mathrm{d}\Gamma \tag{11}$$

where $P_n = n.\nabla P$.

3. DISCRETIZATION FOR THE ROTATING FLOW

When the duct is assumed to be sufficiently long, there is an internal section where the effects at the extremes can be neglected, that is, the flow is fully developed. The axial pressure gradient

$$\frac{\partial P}{\partial z} = -G$$

is considered constant, maintained by external means (P is the modified pressure, which includes the gravitational and centrifugal force potentials). In this situation, it is observed that in the internal region, the physical properties of the flow become independent of the coordinate z, however, the fully developed velocity field is three-dimensional. For non-zero rotation rates, the components u, v of the velocity $\mathbf{v} = (u, v, w)$ are termed the secondary flow and the component w is referred to as the main flow.

With the above considerations, we have the continuity equation

$$\frac{\partial u}{\partial x} + \frac{\partial v}{\partial y} = 0 \tag{12}$$

and the momentum equations

$$\frac{\partial u}{\partial t} + u\frac{\partial u}{\partial x} + v\frac{\partial u}{\partial y} = -\frac{\partial P}{\partial x} + v\nabla^2 u - 2\omega w$$

$$\frac{\partial v}{\partial t} + u\frac{\partial v}{\partial x} + v\frac{\partial v}{\partial y} = -\frac{\partial P}{\partial y} + \nu\nabla^2 v$$

$$\frac{\partial w}{\partial t} + u\frac{\partial w}{\partial x} + v\frac{\partial w}{\partial y} = \frac{G}{\rho} + \nu\nabla^2 w + 2\omega u$$

This model will be employed for determining the secondary flow in a transversal section $(0,D)\times(0,H)$ perpendicular to the axis of the duct as in Figure 1. The aspect ratio is given for $\chi = H/D$. In a non-dimensional form, we have the system

$$\frac{\partial u}{\partial t} + u\frac{\partial u}{\partial x} + v\frac{\partial u}{\partial y} = -\frac{\partial P}{\partial x} + \frac{1}{Re}\nabla^2 u - 2\frac{1}{Ro}w \tag{13}$$

$$\frac{\partial v}{\partial t} + u\frac{\partial v}{\partial x} + v\frac{\partial v}{\partial y} = -\frac{\partial P}{\partial y} + \frac{1}{Re}\nabla^2 v \tag{14}$$

$$\frac{\partial w}{\partial t} + u\frac{\partial w}{\partial x} + v\frac{\partial w}{\partial y} = C + \frac{1}{Re}\nabla^2 w + 2\frac{1}{Ro}u \tag{15}$$

where the non-dimensional constant

$$C = \frac{GD}{\rho W_0^2}$$

corresponds to the form of the longitudinal pressure gradient $-\partial P/\partial z$.

Systems (13)–(15) will be now discretized with finite differences on a staggered grid [3]. Let the transverse section of the duct be divided in $N\times M$ rectangular cells and set

$$x_i = i\Delta x, \qquad y_j = j\Delta y$$

$$x_{i-\frac{1}{2}} = \left(i-\tfrac{1}{2}\right)\Delta x, \quad y_{j-\frac{1}{2}} = \left(j-\tfrac{1}{2}\right)\Delta y$$

$$i = 1,2,\ldots,N; \quad j = 1,2,\ldots,M$$

At each time t, we consider the staggered spatial approximation

$$P_{i,j} \approx P(t, x_{i-\frac{1}{2}}, y_{j-\frac{1}{2}})$$

$$u_{i,j} \approx u(t, x_i, y_{j-\frac{1}{2}})$$

$$v_{i,j} \approx v(t, x_{i-\frac{1}{2}}, y_j)$$

$$w_{i,j} \approx w(t, x_{i-\frac{1}{2}}, y_{j-\frac{1}{2}})$$

The first-order derivatives can be approximated by forward or central differences. The notation $D_{1r}, D_{2r}, r = x, y$ is employed for the first-order forward difference operator and for the second-order difference operator, respectively. For second-order derivatives, D_{xx}, D_{yy} correspond to the respective second-order central difference operators. The pressure gradient will be approximated with a first-order forward difference operator, while the terms with velocity by a second-order central difference operator. Thus

$$\nabla_{[n]}\Phi_{i,j} = (D_{nx}, D_{ny})\Phi_{i,j}, \quad n = 1, 2$$

and

$$\nabla^2_{[2]}\Phi_{i,j} = (D_{xx} + D_{yy})\Phi_{i,j}$$

for the Laplacian, where Φ is an any scalar field.

By using these spatial finite differences approximations, the momentum equation has the semi-discrete approximation

$$\frac{\partial \mathbf{u}_{i,j}}{\partial t} = -\nabla_{[1]}P_{i,j} - \mathbf{u}_{i,j}.\nabla_{[2]}\mathbf{u}_{i,j} + \frac{1}{Re}\nabla^2_{[2]}\mathbf{u}_{i,j} + \mathbf{F}[\mathbf{u}_{i,j}] \tag{16}$$

or, in an expanded way with (13)–(15)

$$\frac{\partial u_{i,j}}{\partial t} = -D_{1x}(P_{i,j}) - u_{i,j}D_{2x}(u_{i,j}) - v|_{u_{i,j}}D_{2y}(u_{i,j}) + \frac{1}{Re}(D_{xx}(u_{i,j}) + D_{yy}(u_{i,j})) - 2\frac{1}{Ro}w|_{u_{i,j}} \tag{17}$$

$$\frac{\partial v_{i,j}}{\partial t} = -D_{1y}(P_{i,j}) - u|_{v_{i,j}}D_{2x}(v_{i,j}) - v_{i,j}D_{2y}(v_{i,j}) + \frac{1}{Re}(D_{xx}(v_{i,j}) + D_{yy}(v_{i,j})) \tag{18}$$

$$\frac{\partial w_{i,j}}{\partial t} = C - u|_{w_{i,j}}D_{2x}(w_{i,j}) - v|_{w_{i,j}}D_{2y}(w_{i,j}) + \frac{1}{Re}(D_{xx}(w_{i,j}) + D_{yy}(w_{i,j})) + 2\frac{1}{Ro}u|_{w_{i,j}} \tag{19}$$

Here

$$u|_{w_{i,j}} = \frac{u_{i,j} + u_{i,j+1}}{2}$$

$$u|_{v_{i,j}} = \frac{u_{i-1,j} + u_{i-1,j+1} + u_{i,j} + u_{i,j+1}}{4}$$

$$v|_{u_{i,j}} = \frac{v_{i,j-1} + v_{i,j} + v_{i+1,j-1} + v_{i+1,j}}{4}$$

$$v|_{w_{i,j}} = \frac{v_{i,j} + v_{i,j+1}}{2}$$

$$w|_{u_{i,j}} = \frac{w_{i,j} + w_{i+1,j}}{2}$$

3.1. Time discretization

There are many available methods for time discretization. In order to reduce the computational cost, the explicit first-order Euler method will be employed. By writing (16) as

$$\frac{\partial \mathbf{u}_{i,j}}{\partial t} = -\nabla_{[1]} P_{i,j} + \mathbf{U}_{i,j} \tag{20}$$

where

$$\mathbf{U}_{i,j} = -\mathbf{u}_{i,j}.\nabla_{[2]}\mathbf{u}_{i,j} + \frac{1}{Re}\nabla^2_{[2]}\mathbf{u}_{i,j} + \mathbf{F}[\mathbf{u}_{i,j}] \tag{21}$$

we have the time approximation scheme

$$\frac{\mathbf{u}^{k+1}_{i,j} - \mathbf{u}^{k}_{i,j}}{\Delta t} = -\nabla_{[1]} P^k_{i,j} + \mathbf{U}^k_{i,j} \tag{22}$$

In component form

$$u^{k+1}_{i,j} = u^k_{i,j} + \Delta t(-D_{1x}(P^k_{i,j}) + U^k_{i,j}), \quad i = 1:N-1,\ j = 1:M \tag{23}$$

$$v^{k+1}_{i,j} = v^k_{i,j} + \Delta t(-D_{1y}(P^k_{i,j}) + V^k_{i,j}), \quad i = 1:N,\ j = 1:M-1 \tag{24}$$

$$w^{k+1}_{i,j} = w^k_{i,j} + \Delta t(-D_{1z}(P^k_{i,j}) + W^k_{i,j}), \quad i = 1:N,\ j = 1:M$$

$$k = 0, 1, \ldots \tag{25}$$

3.2. Discretization at the boundary

In order to attain stability for the Poisson equation for the pressure, we propose the following discretization at the boundary of the domain, which also maintain the second-order of the discretization at all the domain, we use the Taylor theorem to approximate the gradients and Laplacians

At node $(i, 1)$, we define

$$\left(\frac{\partial u}{\partial y}\right)_{i,1} \approx \frac{3u_{i,1} - 4u_\Gamma + u_{i,2}}{3\Delta y} \tag{26}$$

$$\left(\frac{\partial^2 u}{\partial y^2}\right)_{i,1} \approx \frac{10u_{i,2} + 16u_\Gamma - 25u_{i,1} - u_{i,3}}{5\Delta y^2} \tag{27}$$

u_Γ is the known value at the contour.

The gradients and Laplacians at the contours, for example, at node 0 we have

$$\left(\frac{\partial v}{\partial y}\right)_{i,0} \approx \frac{v_{i,2} - 4v_{i,1} + 3v_\Gamma}{2\Delta y} \tag{28}$$

$$\left(\frac{\partial^2 v}{\partial y^2}\right)_{i,0} \approx \frac{2v_\Gamma - 5v_{i,1} + 4v_{i,2} - 2v_{i,3}}{\Delta y^2} \tag{29}$$

The gradients and Laplacians of w approximated at direction y at face $y=0$ has the form

$$\left(\frac{\partial w}{\partial y}\right)_\Gamma \approx \frac{9w_{i,1} - w_{i,2} - 8w_\Gamma}{3\Delta y} \tag{30}$$

$$\left(\frac{\partial^2 w}{\partial y^2}\right)_\Gamma \approx \frac{24w_\Gamma - 40w_{i,1} + 20w_{i,2} - 4w_{i,3}}{5\Delta y^2} \tag{31}$$

$$\left(\frac{\partial w}{\partial y}\right)_{i,1} \approx \frac{w_{i,2} - 4w_\Gamma + 3w_{i,1}}{3\Delta y} \tag{32}$$

$$\left(\frac{\partial^2 w}{\partial y^2}\right)_{i,1} \approx \frac{10w_{i,2} - w_{i,3} - 25w_{i,1} + 16w_\Gamma}{5\Delta y^2} \tag{33}$$

Similarly at opposed faces.

4. DISCRETIZATION OF THE POISSON EQUATION FOR THE PRESSURE

The discretization of the Poisson equation for the pressure of incompressible flows requires special attention. It is required that the solution of Equation (22) satisfies the continuity equation in the interior of the spatial region Ω.

Since the pressure field to be calculated is time-dependent, the discretization of the equation for pressure (9) is performed for an arbitrary but fixed time. This is done in conjunction with the Neumann condition (10) at the boundary Γ.

The pressure field is determined up to an additive constant corresponding to the level of hydrostatic pressure. This can be removed by prescribing the integral relationship $c = \int\int_\Omega P(x, y)\mathrm{d}x\,\mathrm{d}y$, or by a grounding condition at certain point $P(x_0, y_0) = 0$. This later condition will be considered. Thus, for a given discrete solution $P_{i,j}$, although $(P_{i,j} + c)$ is also a solution for any constant c, the grounding condition let us to determine the pressure by choosing $c = 0$.

Equation (22) can be written as

$$\mathbf{u}^{k+1} = \mathbf{u}^k - \Delta t \nabla P^k + \Delta t f(\mathbf{u}^k) \tag{34}$$

where f contains all viscous and convective terms as well as the rotating term $\mathbf{F}$; that is

$$f(\mathbf{u}) = -\mathbf{u}.\nabla\mathbf{u} + \frac{1}{Re}\nabla^2\mathbf{u} + \mathbf{F}$$

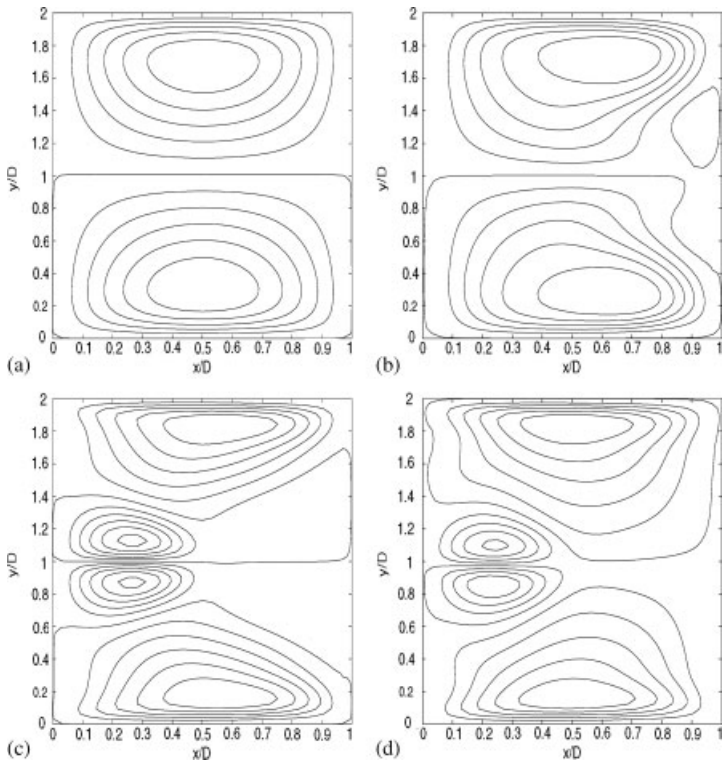

Figure 2. Present work. Streamlines of a secondary flow in a 2:1 duct for t: (a) 1 s; (b) 12.5 s; (c) 75 s; and (d) fully developed. $Re = 279$, $Ro = 1.2$ ($\omega = 0.1$ rad/s, $G = 6 \times 10^{-4}$ lb/ft^3).

Taking divergence in Equation (34), it follows that

$$\nabla.\mathbf{u}^{k+1} = \nabla.\mathbf{u}^{k} - \Delta t \nabla^2 P^{k} + \Delta t \nabla.f(\mathbf{u}^{k}) \tag{35}$$

In order that, at level time $(k+1)$, the continuity equation be satisfied, the condition $\nabla.\mathbf{u}^{k+1} = 0$ must hold. Thus, from Equation (35) turns out the pressure equation

$$\nabla^2 P^{k} = \frac{\nabla.\mathbf{u}^{k}}{\Delta t} + \nabla.f(\mathbf{u}^{k}) \tag{36}$$

The term

$$D_t = \frac{\nabla.\mathbf{u}^{k}}{\Delta t}$$

is called dilatation and it is zero when considering the continuum formulation. Here, this term is maintained with the purpose of eliminating non-linear instabilities [13–15].

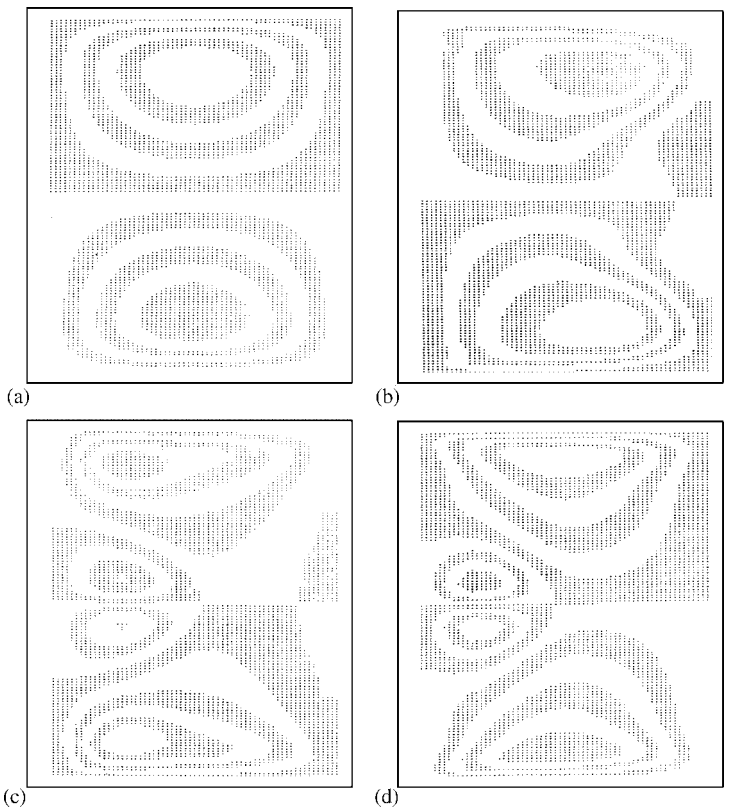

Figure 3. Speziale [5]. Streamlines of a secondary flow in a 2:1 duct for t: (a) 1 s; (b) 12.5 s; (c) 75 s; and (d) fully developed. $Re = 279$, $Ro = 1.2$ ($\omega = 0.1$ rad/s, $G = 6 \times 10^{-4}$ lb/ft^3).

By applying a second-order central difference approximation on a staggered grid, the Poisson equation (36) becomes

$$\nabla^2_{[2]} P_{i,j} = \nabla_{[1]} . \mathbf{U}_{i,j} + D_t \tag{37}$$

where $\mathbf{U}_{i,j}$ is as given in (21).

On the other hand, the continuity equation (12) discretized at the level time $(k+1)$ must be satisfied exactly, that is

$$0 = D_{1x} u^{k+1}_{i-1,j} + D_{1y} v^{k+1}_{i,j-1} \tag{38}$$

Dividing Equation (38) by Δt, we have the dilatation term

$$0 = \frac{D_{1x} u^{k+1}_{i-1,j} + D_{1y} v^{k+1}_{i,j-1}}{\Delta t} = D^{k+1}_t \tag{39}$$

Substituting Equations (23)–(25) in Equation (39), it follows that at each level time k

$$D_{1x} D_{1x} P_{i-1,j} + D_{1y} D_{1y} P_{i,j-1} = D_t + D_{1x} U_{i-1,j} + D_{1y} V_{i,j-1} \tag{40}$$

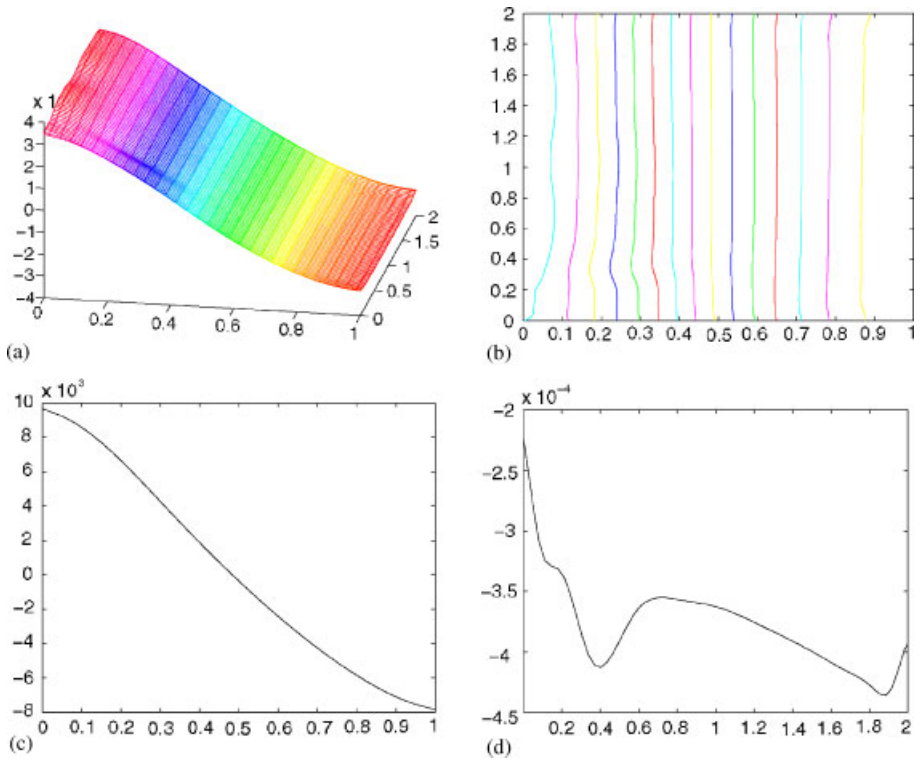

Figure 4. (a) Pressure field; (b) contours; (c) horizontal profile for $y/D = 1$; and (d) vertical profile for $x/D = 0.5$, in a 2:1 duct. $Re = 279$, $C = 0.1345$, $Ro = 1.2$ ($\omega = 0.1$ rad/s, $G = 6 \times 10^{-4}$ lb/ft^3).

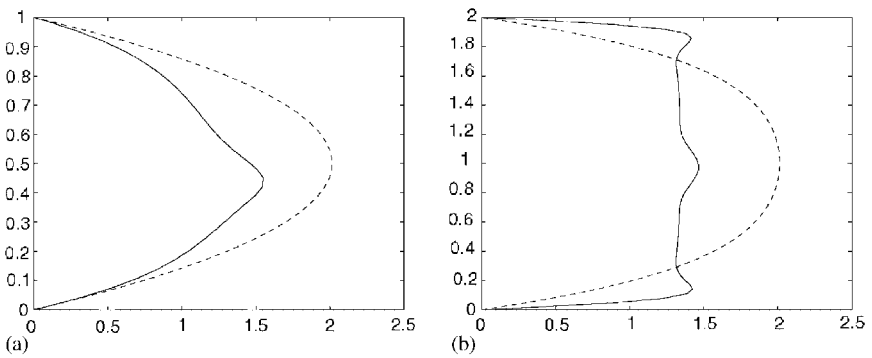

Figure 5. Present work. Axial velocity profiles in a 2:1 duct: (a) horizontal; and (b) vertical, with traced line for $\omega = 0$ and continuous line for $\omega = 0.1$ rad/s, $Re = 279$. Here $Q_f/Q = 0.5429$, $u_{\max}/w_{\max} = 0.15$.

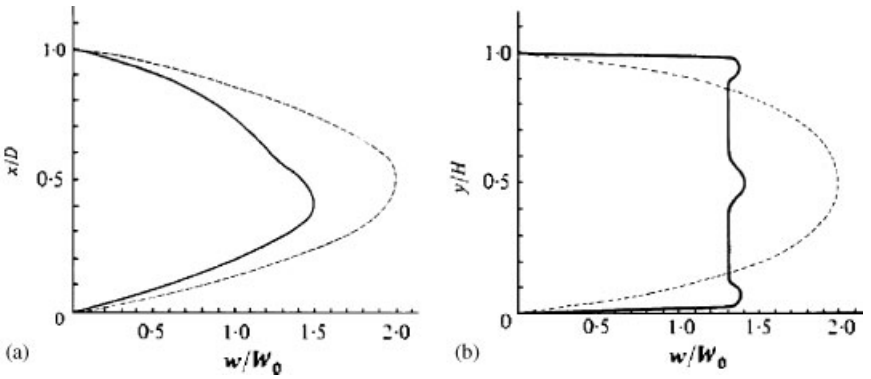

Figure 6. Speziale [5]. Axial velocity profiles in a 2:1 duct: (a) horizontal; and (b) vertical, with traced line for $\omega = 0$ and continuous line for $\omega = 0.1$ rad/s, $Re = 279$, $x/D = \frac{1}{2}$, $y/H = \frac{1}{2}$, $u_{\max}/w_{\max} = 0.19$.

Since the involved operators satisfy $D_{1x}D_{1x}P_{i-1,j} = D_{xx}P_{i,j}$, $D_{1y}D_{1y}P_{i,j-1} = D_{yy}P_{i,j}$, it follows from Equation (40) that

$$\nabla^2_{[2]}P_{i,j} = D_{1x}U_{i-1,j} + D_{1y}V_{i,j-1} + D_t, \quad i = 1:N,\ j = 1:M \tag{41}$$

This is the discretized Poisson equation at level time k.

In order to have a good convergence of the approximate solution of (37), compatibility condition (11) should be satisfied exactly in the discrete form, that is [16, 17]

$$\sum_{i,j\in\Omega} \nabla^2 P_{i,j} = \sum_{i,j\in\Gamma} \frac{\partial P_{i,j}}{\partial n}$$

In fact, by considering $\Delta x = \Delta y = h$ in Equation (41), we have

$$\sum_{i,j=1}^{N,M} P_{i,j-1} + P_{i-1,j} - 4P_{i,j} + P_{i+1,j} + P_{i,j+1}$$

$$= h^2 \sum_{i,j=1}^{N,M} D_t + h \sum_{i,j=1}^{N,M} U_{i,j} - U_{i-1,j} + V_{i,j} - V_{i,j-1} \tag{42}$$

It turns out that

$$\sum_{i=1}^{N} P_{i,0} - P_{i,1} + P_{i,M+1} - P_{i,M} + \sum_{j=1}^{M} P_{0,j} - P_{1,j} + P_{N+1,j} - P_{N,j}$$

$$= h \sum_{i=1}^{N} V_{i,M} - V_{i,0} + \sum_{j=1}^{M} U_{n,j} - U_{0,j} \tag{43}$$

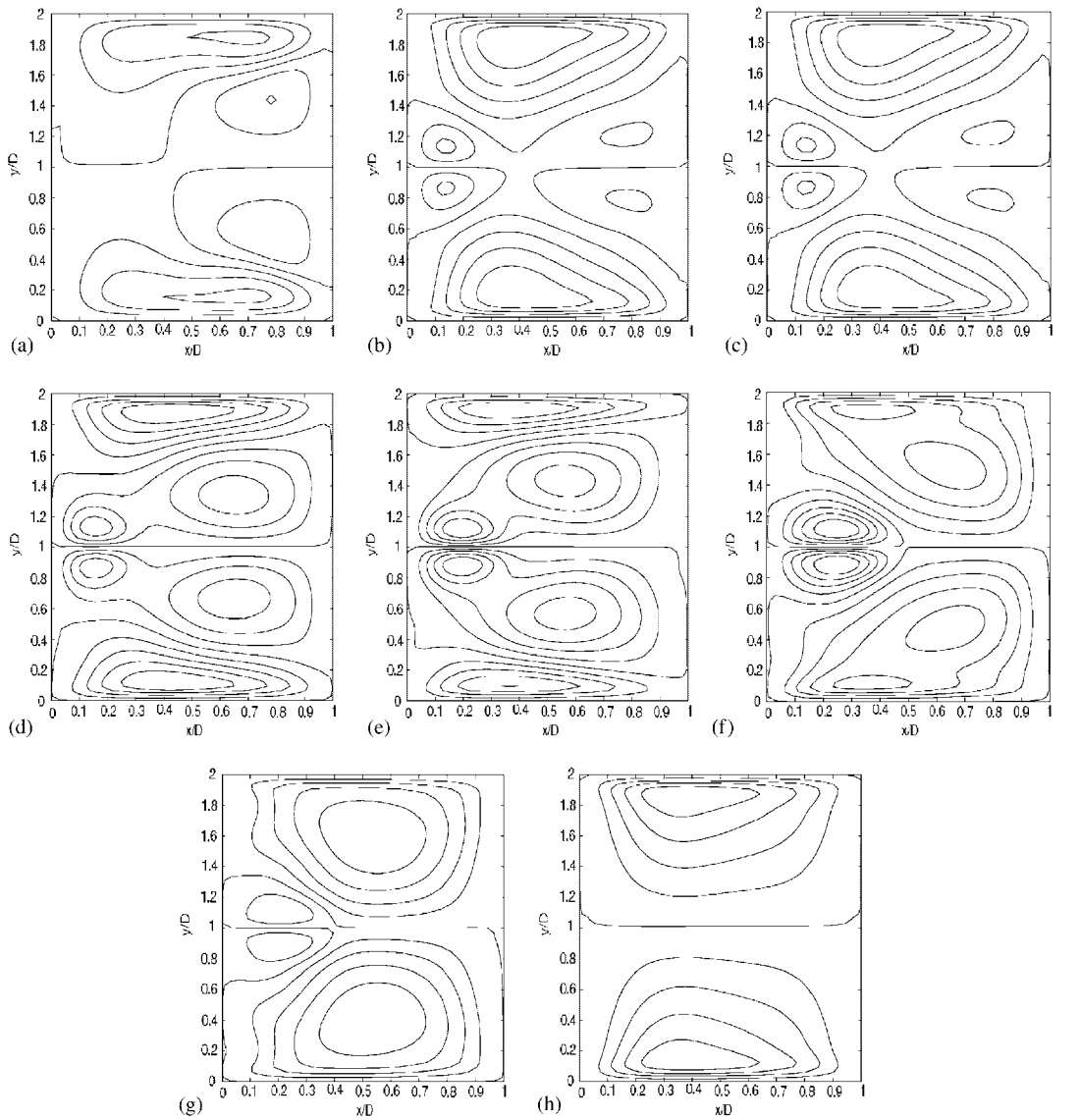

Figure 7. Present work. Streamlines of the secondary flow during instability periods for t: (a) 10 s; (b) 40 s; (c) 45 s; (d) 47 s; (e) 50 s; (f) 55 s; (g) 60 s; and (h) fully developed in a 2:1 duct. $Re = 220$, $Ro = 0.48$ ($\omega = 0.2$ rad/s, $G = 6 \times 10^{-4}$ lb/ft^3).

From the above equation, the discrete Neumann conditions should satisfy the four following relationships:

$$P_{0,j} = P_{1,j} - hU_{0,j}, \quad j = 1, \ldots, M \tag{44}$$

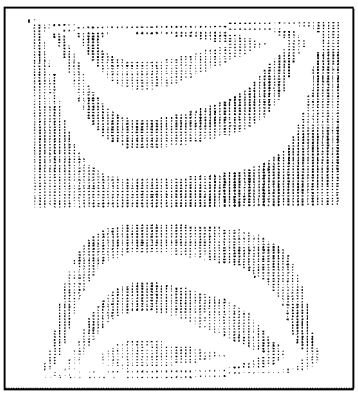

Figure 8. Speziale [5]. Streamlines of the fully developed secondary flow in a 2:1 duct. $Re = 220$, $Ro = 0.48$ ($\omega = 0.2$ rad/s, $G = 6 \times 10^{-4}$ lb/ft^3).

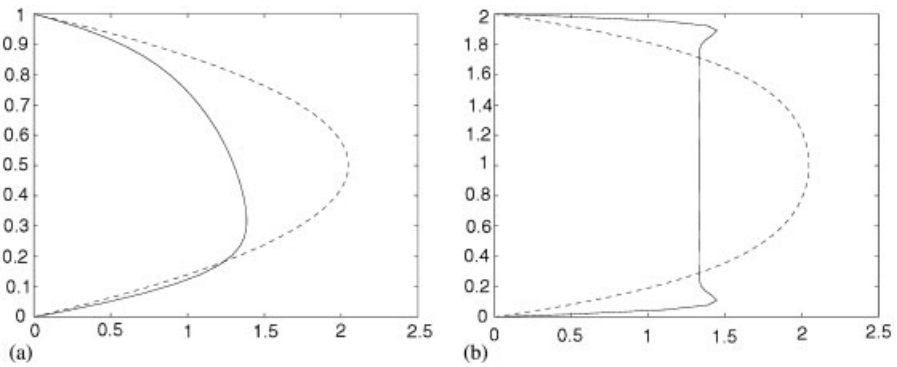

Figure 9. Present work. Fully developed axial velocity profiles in a 2:1 duct: (a) horizontal; and (b) vertical, with traced line for $\omega = 0$ and continuous line for $\omega = 0.2$ rad/s, $Re = 220$. Here $Q_f/Q = 0.4483$, $u_{\max}/w_{\max} = 0.1315$.

$$P_{N-1,j} = P_{N,j} + hU_{N,j}, \quad j = 1, \ldots, M \tag{45}$$

$$P_{i,0} = P_{i,1} - hV_{i,0}, \quad i = 1, \ldots, N \tag{46}$$

$$P_{i,M+1} = P_{i,M} - hV_{i,M}, \quad i = 1, \ldots, N \tag{47}$$

Let us observe that these conditions are a discrete version of Equation (10).

5. A PRESSURE–VELOCITY ALGORITHM

We shall follow an algorithm introduced by Claeyssen *et al.* [2]. At each time level, the pressure is updated in one step and then the velocity field is calculated. The pressure is initialized by solving a singular system that appears from the discretization of the Poisson

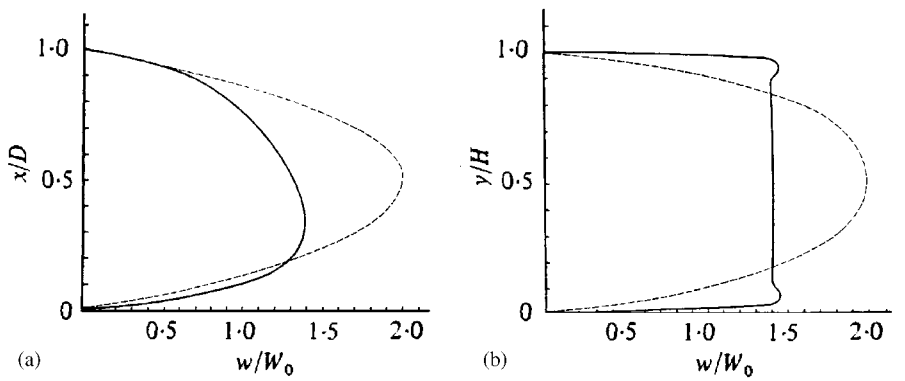

Figure 10. Speziale [5]. Axial velocity profiles in a 2:1 duct: (a) horizontal; and (b) vertical, with traced line for $\omega = 0$ and continuous line for $\omega = 0.2$ rad/s, $x/D = \frac{1}{2}$, $y/H = \frac{1}{2}$, $Re = 220$, $u_{\max}/w_{\max} = 0.13$.

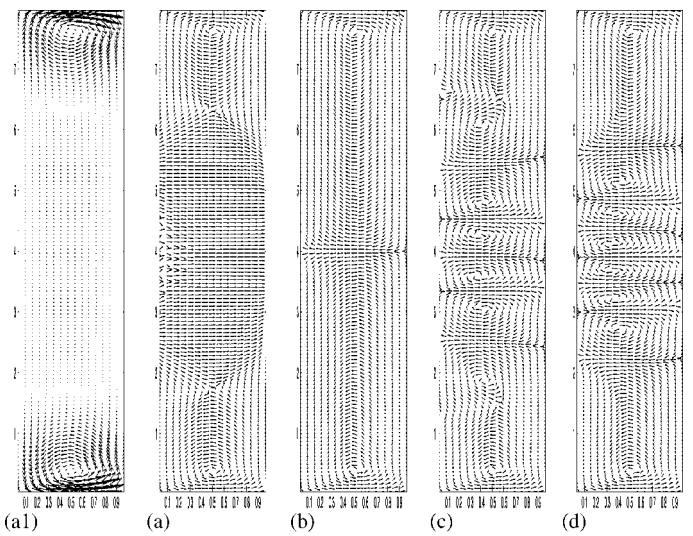

Figure 11. Present work. Secondary flow in an 8:1 duct. (a1) for $t = 10$ s without normalization and normalized for t: (a) 10 s; (b) 500 s; (c) 1600 s; and (d) fully developed. $Re = 248$, $Ro = 21.3$ ($\omega = 0.005$ rad/s, $G = 2 \times 10^{-4}$ lb/ft^3).

equation with a Neumann condition. When solving the Poisson equation, a special treatment is given to the interior points that correspond to the interior cells and to the adjacent cells, in such a way that the compatibility condition is verified. This actualization contains correction terms for a direct computing of the pressure at the interior points of the interior cells. This is done by incorporating the values of the pressure already calculated in neighbouring points. This procedure is described as follows.

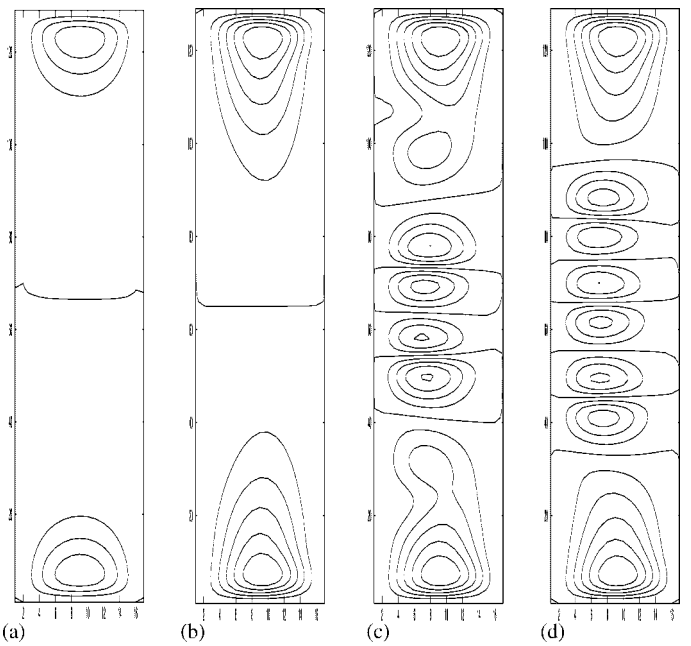

Figure 12. Present work. Streamlines for the secondary flow in an 8:1 duct for t: (a) 10 s; (b) 500 s; (c) 1600 s; and (d) fully developed. $Re = 248$, $Ro = 21.3$ ($\omega = 0.005$ rad/s, $G = 2 \times 10^{-4}$ lb/ft^3).

Let $\mathbf{u} = \mathbf{u}_{i,j}$, and $P = P_{i,j}$. The pressure is initialized by solving the equation

$$\nabla^2_{[2]} P = D_t + \nabla_{[1]} . \left(-\mathbf{u}^k . \nabla_{[2]} \mathbf{u}^k + \frac{1}{Re} \nabla^2_{[2]} \mathbf{u}^k \right) \tag{48}$$

with a SOR method for $k = 0$ [2].

For a direct update of the variables Equation (34) is used.

Let us assume that all discrete variable are known at the time k. We consider $\mathbf{v}^*$ as the velocity that would appear as the solution of Equation (34) with an absent pressure gradient by knowing the field $\mathbf{u}^k$, that is

$$\frac{\mathbf{v}^* - \mathbf{u}^k}{\Delta t_1} = -\mathbf{u}^k . \nabla_{[2]} \mathbf{u}^k + \frac{1}{Re} \nabla^2_{[2]} \mathbf{u}^k + \mathbf{F}[\mathbf{u}^k] \tag{49}$$

Thus

$$\mathbf{v}^* = \mathbf{u}^k + \Delta t_1 \left(-\mathbf{u}^k . \nabla_{[2]} \mathbf{u}^k + \frac{1}{Re} \nabla^2_{[2]} \mathbf{u}^k + \mathbf{F}[\mathbf{u}^k] \right) \tag{50}$$

The variable $\mathbf{v}^*$ is known as *pseudo-velocity* [18], and does not necessarily satisfy the continuity equation. The Helmotz theorem [19, 20] allows to write a finite vector field as the sum of a gradient of a scalar field with a solenoidal vector field, that is, with null divergence. This suggests to write $\mathbf{v}^*$ as the sum of a scalar multiple of the pressure gradient at time

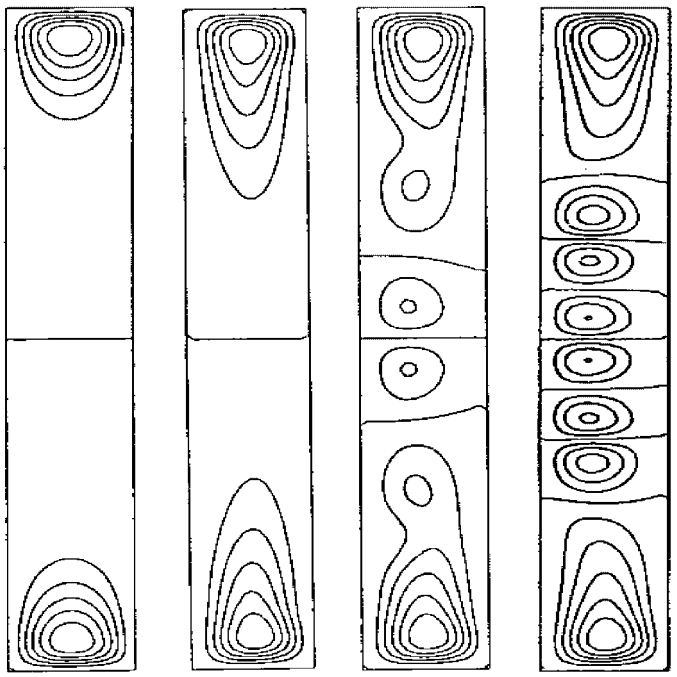

Figure 13. Speziale [6]. Streamlines for the secondary flow in an 8:1 duct for t: (a) 10 s; (b) 500 s; (c) 1600 s; and (d) fully developed. $Re = 248$, $Ro = 21.3$ ($\omega = 0.005$ rad/s, $G = 2 \times 10^{-4}$ lb/ft^3.)

$(k+1)$ and a solenoidal vector field A, that is

$$\mathbf{v}^* = r\nabla P^{k+1} + A \quad \text{such that } \nabla .\, A = 0 \tag{51}$$

Now, defining the velocity at time $(k+1)$ as $\mathbf{u}^{k+1} = A$, and the step of time as $\Delta t = r$, it follows that

$$\mathbf{u}^{k+1} = \mathbf{v}^* - \Delta t \nabla P^{k+1} \tag{52}$$

By substituting (50) in (52), we have the discrete version of (16) with $\Delta t_1 = \Delta t$

$$\frac{\mathbf{u}^{k+1} - \mathbf{u}^k}{\Delta t} = -\nabla_{[1]} P^{k+1} - \mathbf{u}^k . \nabla_{[2]} \mathbf{u}^k + \frac{1}{Re} \nabla^2_{[2]} \mathbf{u}^k + \mathbf{F}[\mathbf{u}^k] \tag{53}$$

Thus, $\mathbf{u}^{k+1}$ is a discrete solution of Equation (16) and satisfies the continuity equation. Now, by taking divergence in (52), it follows that

$$\nabla^2_{[2]} P^{k+1} = \frac{\nabla . \mathbf{v}^*}{\Delta t} \tag{54}$$

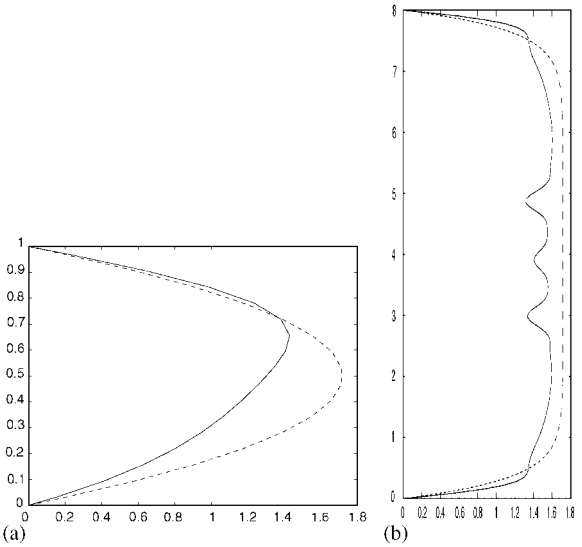

Figure 14. Present work. Axial velocity profiles in an 8:1 duct: (a) horizontal; and (b) vertical. Traced lines for $\omega = 0$ and continuous lines for $\omega = 0.005$ rad/s, $Re = 248$. Here $Q_f/Q = 0.9290$, $u_{\max}/w_{\max} = 0.0287$.

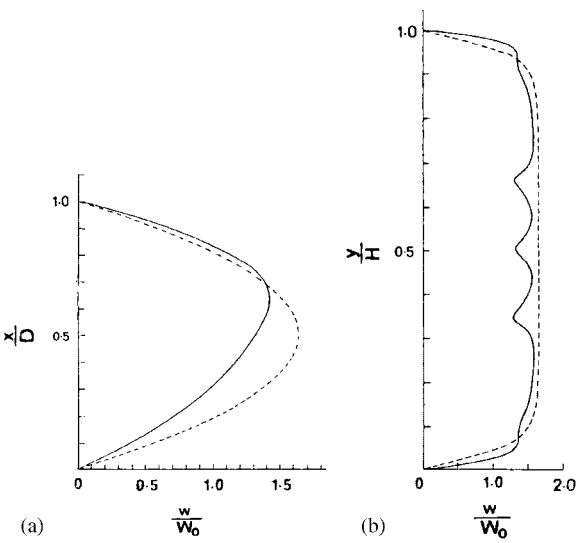

Figure 15. Speziale [6]. Axial velocity profiles in an 8:1 duct: (a) horizontal; and (b) vertical. Traced lines for $\omega = 0$ and continuous lines for $\omega = 0.005$ rad/s, $Re = 248$. $Q_f/Q = 0.924$, $x/D = \frac{1}{2}$, $y/H = 12$.

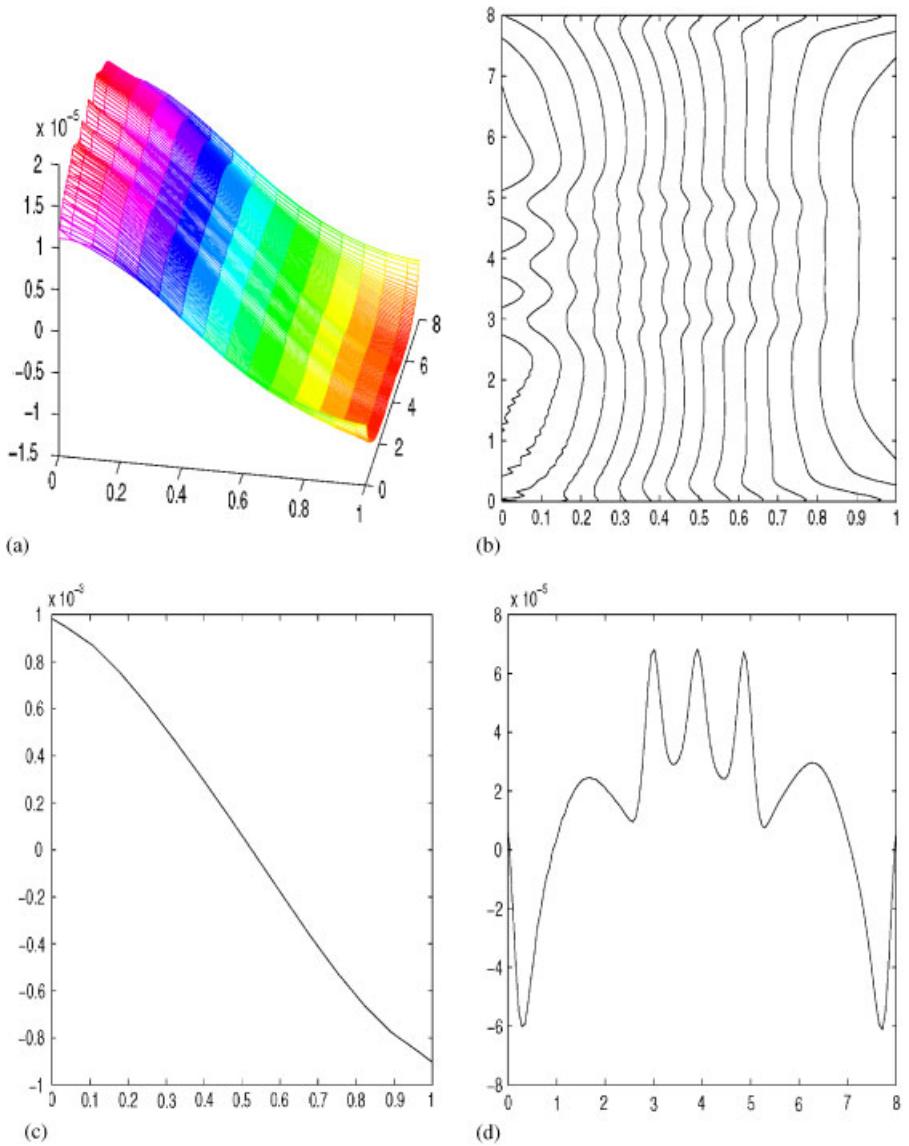

Figure 16. Present work. (a) Pressure field; (b) contours; (c) horizontal profile for $y/D = 4$; and (d) vertical profile for $x/D = 0.5$, in an 8:1 duct. $Re = 248$, $C = 0.0569$, $Ro = 21.3$.

With the substitution of (50) in (54), we arrive to the following discrete equation for the pressure at the level time $(k+1)$

$$\nabla^2_{[2]} P^{k+1} = \frac{\nabla.\mathbf{v}^k}{\Delta t} + \nabla_{[1]}.\left(-\mathbf{u}^k.\nabla_{[2]}\mathbf{u}^k + \frac{1}{Re}\nabla^2_{[2]}\mathbf{u}^k + \mathbf{F}[\mathbf{u}^k]\right)$$
$$= \nabla.\mathbf{U}^k + D_t^k \tag{55}$$

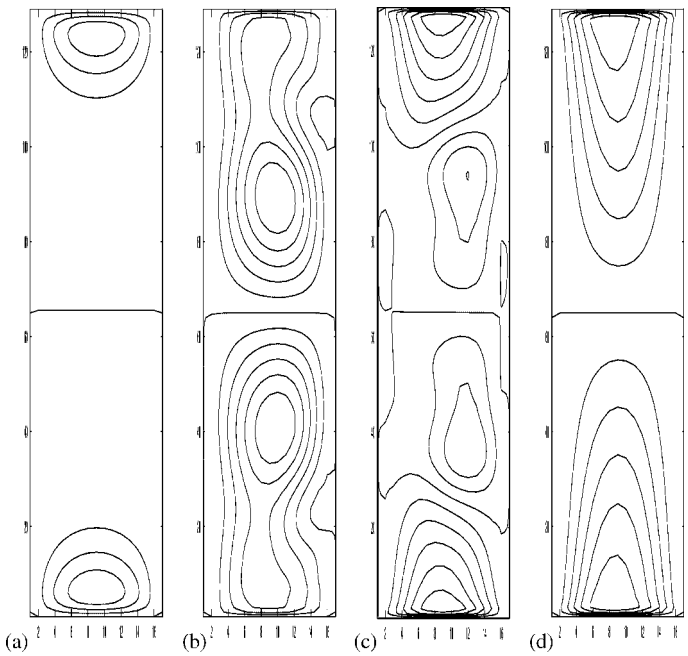

Figure 17. Present work. Streamlines for the secondary flow in an 8:1 duct for t: (a) 1 s; (b) 25 s; (c) 50 s; and (d) fully developed. $Re = 171$, $Ro = 0.3674$ ($\omega = 0.2$ rad/s, $G = 2 \times 10^{-4}$ lb/ft^3).

The fictitious values that appear in the discretization of the Neumann condition (44)–(47), are calculated through the following equations:

$$P_{0,j}^{k+1} = P_{1,j}^{k} - hU_{0,j}^{k}, \quad j = 1, \ldots, M \tag{56}$$

$$P_{N-1,j}^{k+1} = P_{N,j}^{k} + hU_{N,j}^{k}, \quad j = 1, \ldots, M \tag{57}$$

$$P_{i,0}^{k+1} = P_{i,1}^{k} - hV_{i,0}^{k}, \quad i = 1, \ldots, N \tag{58}$$

$$P_{i,M+1}^{k+1} = P_{i,M}^{k} - hV_{i,M}^{k}, \quad i = 1, \ldots, N \tag{59}$$

For the interior points, the pressure field is updated by solving Equation (55) with the incorporation of values already determined, that is, we consider the one step scheme for computing the pressure field

$$P_{i,j}^{k+1} = \tfrac{1}{4}\,(P_{i,j-1}^{k+1} + P_{i-1,j}^{k+1} + P_{i+1,j}^{k} + P_{i,j+1}^{k} + h^2 \nabla_{[1]}\mathbf{U}^{k} + h^2 D_t^{k}) \tag{60}$$

where $\Delta x = \Delta y = h$.

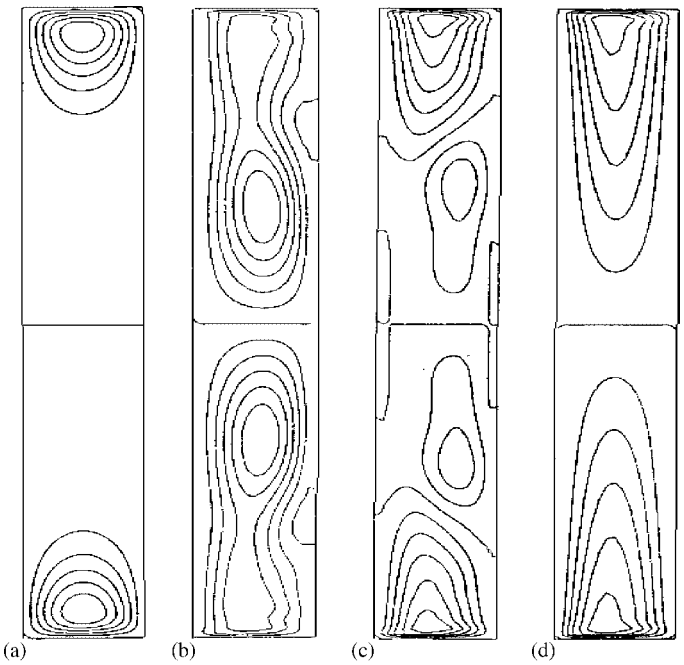

Figure 18. Speziale [6]. Streamlines for the secondary flow in an 8:1 duct for t: (a) 1 s; (b) 25 s; (c) 50 s; and (d) fully developed. $Re = 171$, $Ro = 0.3674$ ($\omega = 0.2$ rad/s, $G = 2 \times 10^{-4}$ lb/ft^3).

5.1. *The pressure–velocity algorithm*

With the above discussion, an algorithm for integrating the Navier–Stokes equations for a rotating flow with a prescribed Neumann condition for the pressure can be formulated as follows:

1. Introduction of the initial velocity, corresponding to the initial time level $k = 0$, the boundary conditions and involved physical parameters;
2. Initialization of the pressure through Equation (48);
3. Calculation of the pseudo-velocity field v^* by using (50);
4. One step up-dating of the pressure field by using (56)–(60);
5. Up-date of the velocity field $\mathbf{u}^{k+1}$ through (52);
6. To do steps (3)–(5) for $k = 1, 2, \ldots$;
7. End the calculations.

6. NUMERICAL SIMULATION RESULTS

In this section, the results of the simulations performed for obtaining the secondary flow by several rotation rates of the duct about a perpendicular axis to it are presented.

As a physical admissible situation, the fully developed flow without rotation was considered and, consequently, as a 1D flow, with velocity field $\mathbf{u} = w_1(x, y)k + 0i + 0j$, where the

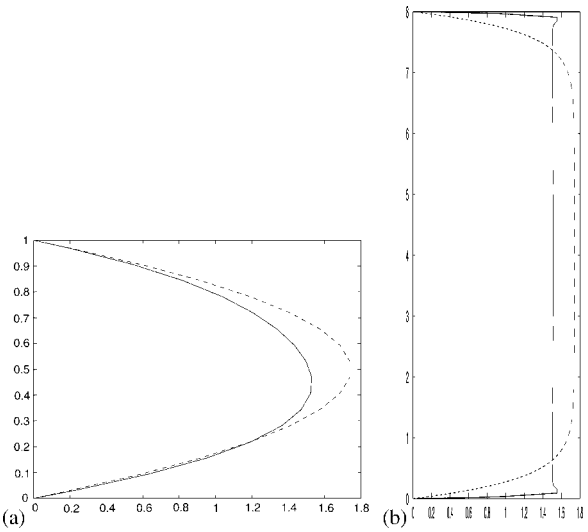

Figure 19. Present work. Axial velocity profiles in an 8:1 duct: (a) horizontal; and (b) vertical. Traced lines for $\omega = 0$ and continuous lines for $\omega = 0.2$ rad/s, $Re = 171$. Here $Q_f/Q = 0.6603$, $u_{\max}/w_{\max} = 0.1529$.

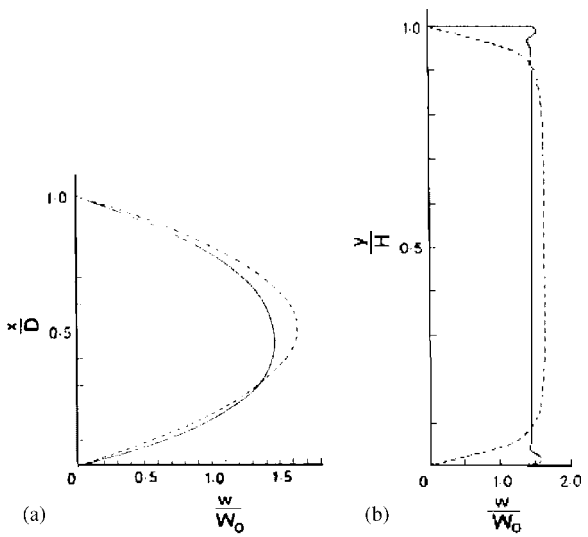

Figure 20. Speziale [6]. Axial velocity profiles in an 8:1 duct: (a) horizontal; and (b) vertical. Traced lines for $\omega = 0$ and continuous lines for $\omega = 0.2$ rad/s, $Re = 171$. $Q_f/Q = 0.636$, $x/D = \frac{1}{2}$, $y/H = 12$.

component w_1 is determined by solving the Poisson equation

$$-\Delta w_1 = Re\, C \tag{61}$$

subject to a non-slip boundary condition $w=0$ on Γ. Thus, w_1 corresponds to a classical quasi-parabolic profile.

Then, in an instant that can be defined as $t=0$, an impulsive angular velocity ω was applied. This allows to consider the initial velocity field conditions

$$u(0)=v(0)=0 \quad \text{and} \quad w(0)=w_1$$

At the walls of the duct, the conditions were prescribed

$$u=0, \quad v=0, \quad w=0$$

For the non-dimensional scaling, the mean velocity of the principal fully developed flow W_0 was employed as velocity scale. The angular velocity ω and the longitudinal pressure gradient $-G$ turn out control parameters for a fixed viscosity $v=1.1\times10^{-5}$ ft^2/s, corresponding to water at an environment mean temperature, and the specific mass $\rho=1.936$ slugs/ft^3. The problem was considered of small scale, because the characteristic length of a duct was the width of the traverse section $D=1.92$ in. The characteristic velocity was chosen as the mean value of the main flow fully developed, consequently, the Reynolds number and the Rossby number were calculated only after the simulation.

A comparison of results was done with the ones obtained by Speziale [5, 6] who employed the vorticity-divergence formulation in contrast with the primitive variables formulation employed in this work.

The simulations were performed for ducts with an aspect ratio 2:1 and ducts with an aspect ratio of 8:1. In the first case, a uniform grid of 32×64 points where $\Delta x=\Delta y=0.005$ ft was considered. For the duct of ratio 8:1 a grid of 16×128 points, where $\Delta x=\Delta y=0.01$ ft was considered. The stability criteria was the usual one, that is, by a superposition of the Courant and Neumann conditions [6]. More specifically, Δt should satisfy the condition

$$\Delta t \leqslant \left[\frac{2}{Re}\left(\frac{1}{\Delta x^2}+\frac{1}{\Delta y^2}\right)+\frac{u_{\max}}{\Delta x}+\frac{v_{\max}}{\Delta y}\right]^{-1} \tag{62}$$

where $u_{\max}$ and $v_{\max}$ are the maximum values of the transversal velocity components.

In what follows, results are exhibited for a transversal section with aspect ratio 2:1.

Figure 2 corresponds to the secondary flow, obtained in this work, for $Re=279$, non-dimensional longitudinal pressure gradient constant $C=0.1345$ ($G=6\times10^{-4}$ lb/ft^3) and Rossby number $Ro=1.2$ (which corresponds to an angular velocity $\omega=0.1$ rad/s). Here, we observe that, in addition to the main vortices, two secondary vortices appear in the mean section of the duct. This phenomena is similar to the one that occurs with curved ducts with rectangular section [7]. In order to effects of comparison, in Figure 3 the correspondents results of Speziale [5] are presented.

In the work of Speziale, the pressure was not calculated within the vorticity-divergence formulation. In this work, the primitive variables formulation is employed and some results for the pressure are obtained. This is illustrated in Figure 4, where the pressure field, the contour lines and the profiles of the central lines of the transverse section are presented. Considering the pressure field, it is observed that in the side more near to the axis of rotation,

called the side of the pressure, the pressure is higher if compared to the opposite side (the suction side).

Figure 5 (present work) and Figure 6 (results of Speziale [5]) present a comparison of the longitudinal velocity profiles, at the horizontal and vertical lines, placed in the centre of the transverse section. The trace lines correspond to the initial longitudinal velocity profiles (without rotation effect, $\omega = 0$). The continuous lines are the fully developed velocity profiles due to the effect of rotation ($\omega = 0.1$ rad/s). It is observed, also, that there is an asymmetry of the longitudinal fully developed velocity profiles in relation to the initial profile, existing a deviation of the maximum of the profile in the direction to the side of higher pressure.

It is clear that a rotation generates a loss of the flowrate in the longitudinal direction in relation to the ratio of the flowrate that is able to carry the primary flow in the absence of rotation. This ratio is defined by Q_f/Q, where Q_f is the end flowrate and Q is the initial flowrate. In this work $Q_f/Q = 0.5429$ and the ratio of the maximum values among the horizontal and the longitudinal components of the velocity field is given by $u_{\max}/w_{\max} = 0.15$.

For a greater angular velocity such as $\omega = 0.2$ rad/s, that is $Ro = 0.48$, $Re = 220$ and $C = 0.2296$, the secondary flow, before reaching the state of fully developed, has periods of instability as it can be observed in Figure 7.

In Figure 7, we observe that the secondary vortices at the centre section are moved to the inferior and superior ends. However, in the period of time $t = 40$ s until $t = 60$ s (Figures 7 (b)–(g)), it can be observed that four vortices at the centre appear, two of which are moved to the ends, and the other two are dissipated at the same centre, when it was reaching the fully developed flow (Figure 7(h)). Approximately at $t = 500$ s, the flow is able to stabilize in two counter-rotating vortices. The results obtained in this work (Figure 7(h)) can be compared with the ones obtained by Speziale [5] (Figure 8).

Figure 9 (present work) and Figure 10 (results of Speziale [5]) illustrate comparisons of the longitudinal velocity profiles of the fully developed flow.

Now we consider a transverse section with aspect ratio 8:1. Figures 11 and 12, exhibit the secondary flow, obtained in this work, for $Ro = 21.3$, $\omega = 0.005$ rad/s. It can be observed that, in the centre of the left side and for time $t = 10$, there is a small disorder, consequence of the rotation. Although, they have a neglecting presence, as one can see, the streamlines do not capture this fact. In Figure 11(a1), the velocity field without normalization is presented for $t = 10$. Here we cannot observe the phenomena exhibit in Figure 11(a), that is, the velocity field, in this portion of the transversal section, is smaller than the fields that appear in the inferior and superior faces. It can be said that the normalized velocity field exhibits more information of what happens in the other portions of the solution domain. This is one of the advantages of working in primitive variables.

In Figure 12 it is observed too that the secondary flow initially assumes a double vortex configuration where each vortex, whose size is the order of the width of the channel, is slightly compressed against the horizontal wall of the channel to which it is adjacent. Then, the stretched double vortex secondary flow becomes unstable so that it becomes a double vortex secondary flow combined with roll-cells in the interior of the channel. In Figure 13 the correspondents results of Speziale [6] are presented.

The present algorithm allows to determine quicker the secondary flow. For instance, a similar structure to the one obtained by Speziale [6] in 1600 s, is obtained by the present algorithm in 750 s. The fully developed flow is qualitatively the same as the one obtained by Speziale.

Figure 14 (present work) and Figure 15 (results of Speziale [6]), exhibit a comparison of the longitudinal velocity profiles. The initial one, without rotation ($\omega = 0$) with a traced line, and the fully developed ($\omega = 0.005$ rad/s) with a continuous line, for the flowrate that decreases in approximately 7.6%. For the same parameters, results, obtained in this work, for the pressure in a state fully developed are given in Figure 16.

For a greater angular velocity such as $\omega = 0.2$ rad/s, that is, $Ro = 0.3674$, $Re = 171$ and $C = 0.1196$ ($G = 2 \times 10^{-4}$ lb/ft^3), the secondary flow restabilizes to a stretched double vortex configuration, as it can be observed in Figure 17(d) (present work) and in Figure 18(d) (results of Speziale [6]). The corresponding velocity profiles are shown in Figure 19 (present work) and in Figure 20 (results of Speziale [6]). For this faster rotating channel, there is a reduction in the flowrate of approximately 37%.

We should mention that all the results showed here, for ducts with aspect ratio 2:1 and 8:1, are in good agreement with those obtained by Speziale [5, 6].

7. CONCLUSIONS

A numerical study of the internal flow of an incompressible viscous fluid in a rectangular duct subject to a rotation force has been developed. Finite differences in primitive variables in a staggered grid with a Neumann condition [1] for the pressure were employed.

Numerical simulations were made for ducts with aspect ratios 2:1 and 8:1, for a wide variety of Reynolds numbers and rotation rates, by using a direct velocity–pressure algorithm [2]. This algorithm solves without any iteration the Poisson equation for the pressure. This equation is time dependent due to the incorporation of the velocity field through the Neumann condition for the pressure.

The results obtained for a duct of aspect ratio 2:1, show the breakdown of the double-vortex secondary flow as well as their effects in the axial flow. For $Re = 279$ and rotation rate $\omega = 0.1$ rad/s ($Ro = 1.2$) it is observed that the secondary flow starts with a double-vortex configuration and then breaks down in a configuration of four counter-rotating vortices that are non-symmetric with respect to the central vertical line of the duct (Figure 2(d)). The resultant secondary flow is very similar to those obtained by Chen *et al.* [7] for curved rectangular dutos. When the angular speed of the duct is increased for $\omega = 0.2$ rad/s ($Re = 220$ and $Ro = 0.48$) it is observed that the subsidiary counter-rotating vortices pair that were on the side of the high pressure of the duct (Figure 2(d)) disappear and the secondary flow restabilizes to a slightly asymmetric double-vortex configuration as shown in Figure 7(h).

For a duto 8:1 with $Re = 248$ and $\omega = 0.005$ rad/s ($Ro = 21.3$), it is observed that the double secondary vortex initially obtained (Figure 12(a)) is replaced with the double vortex secondary flow combined with roll-cells in the interior of the channel (Figure 12(d)). When the angular velocity of the duct is increased to $\omega = 0.2$ rad/s ($Ro = 0.3674$ and $Re = 171$), the secondary flow restabilizes to the stretched double vortex configuration (Figure 17(d)).

The simulations for the ducts of aspect ratio 2:1 and 8:1 were compared with the existent solutions [5, 6], showing a very good agreement.

The numerical scheme developed in this work for a rotating flow could be employed in connection with non-Newtonian fluids and mixed convection problems. They are matter of a future work of the authors.

REFERENCES

1. Gresho PM, Sani RL. On pressure boundary conditions for the incompressible Navier–Stokes equations. *International Journal for Numerical Methods in Fluids* 1987; **7**:1111–1145.
2. Claeyssen JR, Bravo E, Platte R. Simulation in primitive variables of incompressible flow with pressure Neumann condition. *International Journal for Numerical Methods in Fluids* 1999; **30**:1009–1026.
3. Harlow FH, Welch JE. Numerical calculation of time dependent viscous incompressible flow of fluid with free surface. *Physics of Fluids* 1965; **8**:2182–2189.
4. Robertson AM. On viscous flow in curved pipes of non-uniform cross-section. *International Journal for Numerical Methods in Fluids* 1996; **22**:771–798.
5. Speziale CG. Numerical study of viscous flow in rotating rectangular ducts. *Journal of Fluid Mechanics* 1982; **122**:251–271.
6. Speziale CG. *Numerical Solution of Rotating Internal Flows*. Lectures in Applied Mathematics, vol. 22. American Mathematical Society: Providence, RI, 1985; 261–288.
7. Chen HB, Nandakumar K, Finlay WH, Ku HC. Three-dimensional viscous flow through rotating channel: a pseudospectral matrix method approach. *International Journal for Numerical Methods in Fluids* 1996; **23**: 379–396.
8. Yang Z. Large eddy simulation of fully developed turbulent flow in a rotating pipe. *International Journal for Numerical Methods in Fluids* 2000; **33**:681–694.
9. Govatsos PA, Papantonis DE. A characteristic based method for the calculation of three-dimensional incompressible, turbulent and steady flows in hydraulic turbomachines and installations. *International Journal for Numerical Methods in Fluids* 2000; **34**:1–30.
10. Hart JE. Instability and secondary motion in a rotating channel flow. *Journal of Fluid Mechanics* 1971; **45**: 341–351.
11. Ladyzhenskaya O. *The Mathematical Theory of Viscous Incompressible Flow*. Gordon and Breach: New York, 1969.
12. Sheu TWH, Wang MMT, Tsai SF. Pressure boundary condition for a segregated approach to solving incompressible Navier–Stokes equations. *Numerical Heat Transfer*, *Part B* 1998; **34**:457–467.
13. Roache PJ. *Computational Fluid Dynamics*. Hermosa Publishers: Albuquerque, NM, 1982.
14. Ames WF. *Numerical Methods for Partial Differential Equations* (3rd edn). Academic Press: New York, 1992.
15. Ferziger JH, Perić M. *Computational Methods for Fluid Dynamics* (2nd edn). Springer: Berlin, 1999.
16. Abdallah S. Numerical solutions for the pressure Poisson equation with Neumann boundary conditions using a non-staggered grid. *Journal of Computational Physics* 1987; **70**:182–192.
17. Alfrink BJ. On the Neumann problem for the pressure in a Navier–Stokes model. *Proceedings of the 2nd International Conference on Numerical Methods in Laminar and Turbulent Flow*, Venice, 1981; 389–399.
18. Nonino C, Comini G. An equal-order velocity–pressure algorithm for incompressible thermal flows. Part 1: formulation. *Numerical Heat Transfer*, *Part B* 1997; **32**:1–15.
19. Morse PM, Feschbach H. *Methods of Theoretical Physics*, *Part I*. McGraw-Hill: New York, 1953.
20. Temam R. *Navier–Stokes Equations* (3rd edn). North-Holland: Amsterdam, 1985.

